IEEE Robotics and Automation Letters (RA-L) paper, presented at ICRA 2024, Yokohama, Japan. Cite as RA-L paper.

Dual-Mode Human-Robot Collaboration with Guaranteed Safety Using Time-Varying Zeroing Control Barrier Functions and Quadratic Program

Kaige Shi and Guoqiang Hu

***Abstract*—Safety and efficiency are two important aspects of human-robot collaboration (HRC). Most existing control methods for HRC consider either contactless HRC or physical HRC, hindering more efficient HRC. The proposed control framework enables dual-mode HRC, filling the gap between contactless and physical HRCs. With the framework, the robot can perform contactless HRC under safety regulations regarding the co-working human. Meanwhile, the human can safely interrupt the robot via physical contact to enter physical HRC, in which he/she can hand guide the robot or take over its gripped object. First, human safety is defined as bounded approaching velocities between human and multiple robot links based on ISO/TS 15066, allowing gradual establishing of physical contact. Then, the time-varying zeroing control barrier function is proposed and defined to guarantee the bounded approaching velocities by a safety control set. Second, a unified task control set is designed to achieve different robot tasks for different HRC modes in a unified manner. The unified task control set enables the robot to switch smoothly between the two HRC modes. An optimal final control input is determined by a quadratic program based on different control sets. Experiments were conducted to verify the proposed framework and compare the proposed framework with existing methods. An application example is presented to show the versatility of the proposed framework.**

***Index Terms*— Control barrier function, human safety, physical human-robot collaboration, quadratic program.**

I. Introduction

RECENT developments in robot technology enable humans and robots to work side by side in a shared workspace. Human safety is still an important topic in human-robot collaboration (HRC). It arises from many aspects of HRC. For example, the human may be hit by the robot's structure or something mounted to the end-effector (EE), and imperfect sensing may also cause dangers. The former is usually solved by collision avoidance, while the latter may be solved by novel sensing methods or a sufficient safety margin.

There are generally two modes of HRC, i.e., contactless HRC and physical HRC. In contactless HRC (see Fig. 1(a)), the robot performs its task while avoiding collisions with co-working humans in the same workspace. Different methods, e.g., artificial potential field [1, 2] and optimization program [3-6], are employed to achieve collision avoidance, thereby ensuring human safety. In physical HRC (see Fig. 1(b)), the robot conducts a common task, e.g., co-manipulation [7], co-transportation [8, 9], co-assembly [10], and handover [11], with the human in presence of physical interaction. The robot's motion can be adaptive to the human by employing, e.g., impedance control [7, 9] and trajectory deformation [12], so that the interaction force is safe for the human.

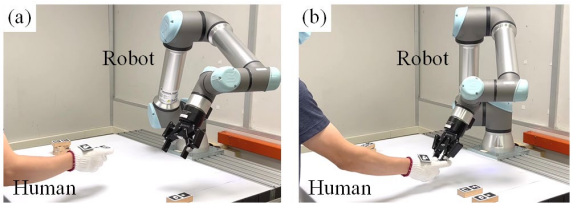

Fig. 1. Demonstration of (a) contactless HRC and (b) physical HRC.

Although some methods capable of both HRC modes have been developed [1, 13, 14], it is still a challenge to switch safely and efficiently between two HRC modes. In contactless HRC mode, the robot should operate at full speed to ensure efficiency. To enter physical HRC mode, the human has to establish physical contact with the operating robot, which may lead to an unsafe human-robot collision. Considering that a large impact force can be produced within the robot's response time, it will be difficult to alleviate the unsafe collision in the physical HRC mode. Therefore, human safety should be considered beforehand in contactless HRC mode. In [1], the mode switching is not presented. In [13], human safety is neglected which may make the mode switching unsafe. In [14], the robot has to stop before switching to physical HRC mode, which may sacrifice efficiency.

In this letter, we propose a control framework capable of both HRC modes with guaranteed human safety. Here, human safety means a limited contact force resulting from a collision with the robot. With this framework, the robot can perform contactless HRC efficiently while fulfilling safety regulations regarding the human. The safety regulations do not stop the robot so that the efficiency of HRC can be maximized. Meanwhile, the human can safely interrupt the robot through physical contact to enter physical HRC mode, in which he/she can guide the robot to a goal position. The robot returns to contactless HRC mode automatically after the human retracts

This research is supported by the National Research Foundation, Singapore under its Medium Sized Center for Advanced Robotics Technology Innovation. *(Corresponding author: Guoqiang Hu.)*

The authors are with the School of Electrical and Electronic Engineering, Nanyang Technological University, Singapore 639798 (e-mail: kaige.shi@ntu.edu.sg; gqhu@ntu.edu.sg).

IEEE Robotics and Automation Letters (RA-L) paper, presented at ICRA 2024, Yokohama, Japan. Cite as RA-L paper.

from the robot. The contribution of this letter is twofold.

First, human safety is defined as bounded approaching velocities between human and multiple robot links based on the ISO/TS 15066 [15]. In [16-18], the regulations in the ISO/TS 15066 are used to avoid human-robot collisions in contactless HRC mode without considering physical HRC. On the contrary, in this letter, the human safety defined by bounded approaching velocities allows safe human-robot collisions, which are desired when the robot switches to physical HRC mode. To guarantee the defined human safety, a novel control barrier function (CBF) called time-varying zeroing CBF (TV-ZCBF) is proposed. Traditional CBFs are time-invariant [19] and thus cannot deal with the time-varying velocity boundary here. Compared to reciprocal CBFs that are undefined in unsafe states [3, 20], zeroing CBFs (e.g., those in [6, 19] and the TV-ZCBF) can deal with safety violations.

Second, a unified task control set is designed to achieve different robot tasks in a unified manner. In contactless HRC, the robot's task is to make its EE track the desired trajectory. In physical HRC, the robot's task is to lead the EE to the human's goal position which is unknown to the robot. The unified task control set enables the robot to switch smoothly between the two HRC modes. A quadratic program (QP) based on the safety control set and the unified task control set is employed to determine the optimal final control input.

The advantages of the proposed framework are as follows: (1) the human-robot approaching velocity is strictly constrained by TV-ZCBFs, thereby limiting the contact force and guaranteeing human safety; (2) the robot is allowed to operate near the human while fulfilling the velocity boundary depending on the human-robot distance, which maximizes HRC efficiency; (3) the robot tasks in different HRC modes are handled in a unified manner, enabling smooth switch of HRC mode.

The rest of this letter is organized as follows. In Section II, the system is modeled and the problem is stated. In Section III, the control framework is constructed. In Section IV, experiments are presented and analyzed. Finally, Section VI concludes this letter.

II. System Modeling and Problem Statement

A. Modeling of Robot and Human

In this letter, we consider the following joint-space dynamics of a robot manipulator with n-DOFs

$$M(q)\ddot{q} + C(q,\dot{q})\dot{q} + G(q) = \tau + J_v^T(q)F_h + J_\omega^T(q)T_h \quad (1)$$

where $q \in \mathbb{R}^n$ is the vector of joint positions, $M \in \mathbb{R}^{n\times n}$ is the symmetric and positive definite inertia matrix, $C \in \mathbb{R}^{n\times n}$ is the Coriolis and centrifugal matrix, $G \in \mathbb{R}^n$ is the gravity vector, $\tau \in \mathbb{R}^n$ is the vector of torque control inputs, $F_h \in \mathbb{R}^3$ and $T_h \in \mathbb{R}^3$ are the vectors of forces and torques by the human at the EE, respectively, and $J_v \in \mathbb{R}^{3\times n}$ and $J_\omega \in \mathbb{R}^{3\times n}$ are linear and angular Jacobian matrices of the EE, respectively. For a commercial robot, the control input τ is bounded, i.e.,

$$\tau \in \mathcal{T} \triangleq \{\tau \in \mathbb{R}^n \mid \tau_{\min} \le \tau \le \tau_{\max}\} \quad (2)$$

where $\tau_{\min} \in \mathbb{R}^n$ and $\tau_{\max} \in \mathbb{R}^n$ are lower and upper bounds of τ, respectively. The robot dynamics (1) can be written in the following control affine form

$$\dot{x} = f(x) + g(x)\tau \quad (3)$$

where $x = [q^T, \dot{q}^T]^T \in \mathbb{R}^{n_x}$ with $n_x = 2n$ is the robot state vector, and $f(x) = [\dot{q}^T, (-M^{-1}(C\dot{q} + G - J_v{}^T F_h - J_\omega{}^T T_h))^T]^T \in \mathbb{R}^{n_x}$ and $g(x) = [0_{n\times n}, -M^{-1}]^T \in \mathbb{R}^{n_x\times n}$ are locally Lipschitz continuous functions.

To facilitate the robot controller design and the system stability analysis, an explicit model of the human is necessary. In this letter, it is assumed that the human applies the force F_h according to the following law in order to guide the robot's EE to his/her goal position [21]

$$F_h = -K_{hP}(p_e - p_g) - K_{hD}\dot{p}_e \quad (4)$$

where K_{hP} and K_{hD} are proportional and derivative gain matrices, respectively, $p_e \in \mathbb{R}^3$ is the position of the robot's EE, and $p_g \in \mathbb{R}^3$ is the human's goal position which is unknown to the robot. The force model (4) is a simplification and is not a predictor of human action. In this letter, the goal position is assumed to be static, i.e., p_g is constant. The human does not intend to rotate the EE, so $T_h \approx 0_{3\times 1}$. Furthermore, F_h and T_h are assumed to be known by the robot. In practical applications, F_h and T_h can be either measured by a force and torque sensor [7, 8] or estimated by an observer [9].

B. Definition of Human Safety

As shown in Fig. 2, a serial robot manipulator is represented by n_r links $p_{r,i}p_{r,i+1}$ with $i \in \{1,\cdots,n_r\}$. Each link can be enveloped by a capsule with radius $r_{r,i}$ centered at $p_{r,i}p_{r,i+1}$. The hands are the most important part of the human and the riskiest part to be hit by the robot. Therefore, in this letter, the human is represented by one of his/her hands enveloped by a sphere with radius r_h centered at p_h. More parts of the human can be included by defining more spheres attached to the human. We use $d_i(x, t)$ to denote the minimum distance between the sphere at p_h and the capsule at $p_{r,i}p_{r,i+1}$. The

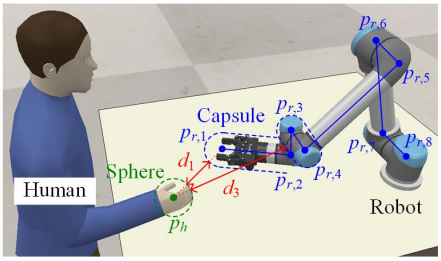

Fig. 2. Geometry of human and robot.

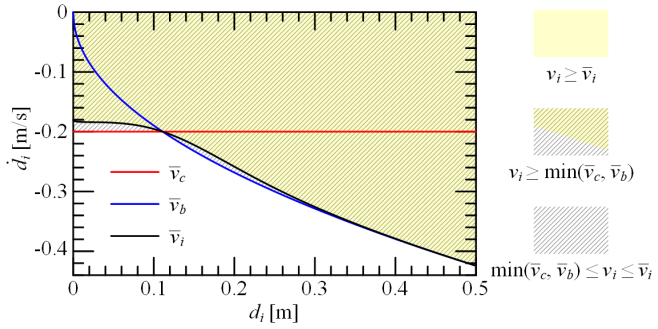

Fig. 3. Velocity boundaries for human safety. The original safe operating region $v_i \ge \min(\bar{v}_c, \bar{v}_b)$ is represented by the shaded area. The modified safe operating region $v_i \ge \bar{v}_i$ is represented by the yellow area.

minimum distance can be calculated as

$$d_i(x,t) = f_d\left(p_h(t), p_{r,i}(x), p_{r,i+1}(x)\right) - r_{r,i} - r_h \quad (5)$$

where f_d: $(\mathbb{R}^3, \mathbb{R}^3, \mathbb{R}^3) \to \mathbb{R}$ is a continuous function giving the minimum distance between a point (i.e., p_h) and a line segment (i.e., $p_{r,i}p_{r,i+1}$). In contactless HRC, human safety is achieved by keeping d_i above a safe distance [2-5]. In this case, the human and the robot are physically separated, which is undesired in dual-mode HRC. To define the human safety in dual-mode HRC, we consider the approaching velocity v_i between the human's hand and the robot's i-th link, which is simply the time derivative of d_i, i.e.,

$$v_i(x,t) = \dot{d}_i(x,t) \quad (6)$$

Note that positive v_i means the human's hand leaves the robot's link, which is safe. While negative v_i means the human's hand approaches the robot's link. In this case, for human safety, v_i should be above a negative lower boundary $\bar{v}_i$. Therefore, in the next, the velocity boundary $\bar{v}_i$ will be determined under the guidance of the ISO/TS 15066 [15].

The technical specification ISO/TS 15066 suggests setting bounds for the robot's velocity to limit the maximum contact force and transferred energy resulting from a hypothetical human-robot collision [15]. The relationships among the maximum contact force F_c, the transferred energy E_c, and the colliding velocity v_c of a collision are as follows

$$E_c = F_c^2/(2k) = m_e v_c^2/2 \quad (7)$$

where k is the stiffness of colliding region of the human's body, and m_e is the effective mass of the system calculated as

$$m_e = (m_h^{-1} + m_r^{-1})^{-1} \quad (8)$$

with m_h and m_r the effective masses of the human and the robot, respectively. The maximum contact force F_c, the stiffness k, and the effective mass m_h depend on the colliding part of the human's body, and their values for different parts have been tabulated in Tables A.2 and A.3 of [15]. The effective mass m_r of the robot can be calculated based on equation (A.4) of [15]. When a human-robot collision is imminent, $\bar{v}_i$ should be above the following colliding velocity boundary to limit the contact force

$$\bar{v}_c = -F_c/\sqrt{m_e k} \quad (9)$$

When d_i is small, i.e., a collision is imminent, it is necessary to adhere to the constant colliding velocity boundary $\bar{v}_c$. However, when d_i is sufficiently large, this boundary is not necessary. In this case, the human is thought to be safe as long as d_i is greater than the robot's braking distance d_b

$$d_b = v_i^2/(2a_b) \quad (10)$$

where a_b is the robot's maximum acceleration depending on the robot's configuration. To be conservative, the following optimization program is employed to determine the value of a_b within a given workspace

$$\begin{aligned} a_b = \min_q & (\|J_v(q)\| \|\ddot{q}_{\max}\|) \\ \text{s.t.} \quad & p_{\min} \le p_e(q) \le p_{\max} \end{aligned} \quad (11)$$

where $\ddot{q}_{\max} \in \mathbb{R}^n$ is the maximum joint acceleration of the robot, and $p_{\min} \in \mathbb{R}^3$ and $p_{\max} \in \mathbb{R}^3$ are the lower and upper boundaries of the robot's workspace, respectively. The maximum acceleration a_b obtained by (11) ensures that it can be reached in any position of the robot's workspace. To ensure $d_i \ge d_b$, the braking velocity boundary should be fulfilled

$$\bar{v}_b(d_i) = -\sqrt{2a_b d_i} \quad (12)$$

The colliding velocity boundary $\bar{v}_c$ and the braking velocity boundary $\bar{v}_b$ are plotted against the human-robot distance d_i in Fig. 3. The velocity boundary $\bar{v}_i$ can be selected as $\min(\bar{v}_c, \bar{v}_b(d_i))$, and the corresponding safe operating region similar to [6] is indicated by the shaded area in Fig. 3. However, in this case, $\dot{\bar{v}}_i$ is not continuous when $\bar{v}_i$ switches between $\bar{v}_c$ and $\bar{v}_b$. This discontinuity is undesired when formulating the TV-ZCBF. To formulate a continuous TV-ZCBF, the following smooth function is adopted for $\bar{v}_i$

$$\bar{v}_i(d_i) = \frac{\bar{v}_c + \bar{v}_b(d_i)}{2} - \frac{\bar{v}_c - \bar{v}_b(d_i)}{2}\tan\frac{d_i - \bar{v}_c^2/(2a_b)}{\epsilon} \quad (13)$$

where $\epsilon = 0.1$ is a constant. In this case, $\bar{v}_i(d_i) \ge \min(\bar{v}_c, \bar{v}_b(d_i))$ holds $\forall d_i \in \mathbb{R}$. As shown in Fig. 3, the modified safe operating region based on (13) (i.e., the yellow area) is a subset of the original safe operating region. Therefore, in dual-mode HRC, human safety can be defined as $v_i \ge \bar{v}_i$.

C. Problem Statement

The problem to be solved in this letter is stated as follows:

1) The human safety defined in Section II.B (i.e., $v_i \ge \bar{v}_i$) should always be fulfilled as a priority.
2) In contactless HRC, the robot's EE should track its desired trajectory to complete the robot's task.
3) In physical HRC, the robot's EE should converge to the human's goal position to achieve hand-guiding.

Next, a control framework will be proposed to achieve the three subproblems. The first subproblem will be achieved by a safety control set based on TV-ZCBFs, while the other two will be achieved by a unified task control set.

III. Control Framework for Dual-Mode HRC

A. Design of TV-ZCBF

A time-varying smooth function $h(x,t)$ dependent on the robot state x and time t is exploited to represent human safety, i.e., $h(x,t) \ge 0$ means the robot state x is safe for the human, while $h(x,t) < 0$ means unsafe. Then, the set of safe robot states $\mathcal{X}$ and its boundary $\partial\mathcal{X}$ can be defined as

$$\begin{cases} \mathcal{X}(t) = \{x \in \mathbb{R}^{n_x} \mid h(x,t) \ge 0\} \\ \partial\mathcal{X}(t) = \{x \in \mathbb{R}^{n_x} \mid h(x,t) = 0\} \end{cases} \quad (14)$$

In the dual-mode HRC, the velocity boundary $\bar{v}_i$ depends on the human-robot distance d_i which further changes with time, so the CBF should be time-varying. For this reason, traditional time-invariant CBFs depending on only the state x cannot be applied here [19]. Furthermore, the reciprocal CBFs [3, 20] that grow to infinity on the boundary $\partial\mathcal{X}$ and are undefined outside of $\mathcal{X}$ may have problems in practical applications, so we adopt the zeroing CBF [6, 19] that is zero on the boundary $\partial\mathcal{X}$ and negative outside $\mathcal{X}$.

Definition 1: Consider the system (3), given the safe set $\mathcal{X}$ in (14), a $\mathcal{C}^1$ function h: $\mathbb{R}^{n_x} \to \mathbb{R}$ is called a TV-ZCBF if there exists a positive constant λ, such that

$$\sup_{\tau \in \mathcal{T}} [A_h \tau + a_h] \ge 0, \quad \forall x \in \mathcal{X} \quad (15)$$

where $A_h = \mathcal{L}_g h$, $a_h = \mathcal{L}_f h + \partial h/\partial t + \lambda h$.

Here, $\mathcal{L}_\bullet h = \partial h/\partial x \cdot \bullet$ is Lie derivative, and $\mathcal{C}^k$ is the set of k times continuously differentiable functions. Once a TV-ZCBF is defined, the admissible control set can be determined as

$$\mathcal{T}_h = \{\tau \in \mathcal{T} \mid A_h\tau + a_h \geq 0\} \tag{16}$$

Theorem 1: If a $\mathcal{C}^1$ function h is a TV-ZCBF, then there exists $\rho(t)$ exponentially converging to 0, such that any controller τ: $\mathbb{R}^{n_x} \to \mathcal{T}_h$ keeps x within a relaxed safe set

$$\mathcal{X}_r(t) = \{x \in \mathbb{R}^{n_x} \mid h(x,t) + \rho(t) \geq 0\} \tag{17}$$

Proof: Note $\dot{h} = \mathcal{L}_g h \cdot \tau + \mathcal{L}_f h + \partial h/\partial t$, $\tau \in \mathcal{T}_h$ implies $\dot{h} + \lambda h \geq 0$. Choose a positive definite function

$$V_h = S^2(h)/2$$

where $S(\bullet) = \min(\bullet, 0)$. Note $S(h) \leq h$ and $S(h) \leq 0$ $\forall h \in \mathbb{R}$. When $h > 0$, $V_h = 0$ and $\dot{V}_h = 0$; when $h \leq 0$, $\dot{V}_h = h\dot{h} \leq -\lambda h^2$. Thus, $\dot{V}_h \leq -2\lambda V_h$ $\forall h \in \mathbb{R}$, implying $V_h(t) \leq V_h(0)e^{-2\lambda t}$. Further, $h(t) \geq S(h) \geq -|S(h(0))|e^{-\lambda t}$. Therefore, there exists $\rho(t) = |S(h(0))|e^{-\lambda t}$ that exponentially converges to 0. ■

The features of the TV-ZCBF are summarized as follows.

- It is a function of the robot state x and the time t, making it adaptive to describe various safety issues including that defined in Section II.B.
- The admissible control set $\mathcal{T}_h$ bases only on the TV-ZCBF's derivatives $\mathcal{L}_g h$, $\mathcal{L}_f h$, and $\partial h/\partial t$, which can be obtained following a standard procedure.
- The TV-ZCBF is guaranteed to be positive as long as the robot's control input is within the admissible control set $\mathcal{T}_h$.

B. Safety Control Set for Human Safety

The following function is a candidate of TV-ZCBF that guarantees human safety in terms of the robot's i-th link

$$h_i(x,t) = v_i(x,t) - \bar{v}_i\big(d_i(t)\big) \tag{18}$$

It is simply the difference between the approaching velocity v_i and the velocity boundary $\bar{v}_i$, so $v_i \geq \bar{v}_i$ is guaranteed as long as h_i is positive. Here, each TV-ZCBF h_i constrains the approaching velocity toward a link of the robot. While in [6], only the approaching velocity toward the EE is constrained using many time-invariant CBFs. The admissible control set that keeps h_i positive is as follows

$$\mathcal{T}_i = \{\tau \in \mathcal{T} \mid A_i\tau + a_i \geq 0\} \tag{19}$$

where $A_i = \mathcal{L}_g h_i$, and $a_i = \mathcal{L}_f h_i + \partial h_i/\partial t + \lambda h_i$. The Lie derivatives and time derivative of h_i are given as follows

$$\mathcal{L}_g h_i = J_{r,i} M^{-1} \tag{20}$$

$$\mathcal{L}_f h_i = J_{r,i} M^{-1}(C\dot{q} + G - J_v^T F_h - J_\omega^T T_h) + \dot{J}_{r,i}\dot{q} \tag{21}$$

$$\partial h_i/\partial t = J_h \ddot{p}_h + \dot{J}_h \dot{p}_h - \bar{v}_i'(d_i) v_i \tag{22}$$

where $J_{r,i} = (\partial f_d/\partial p_{r,i})\cdot(\partial p_{r,i}/\partial q) + (\partial f_d/\partial p_{r,i+1})\cdot(\partial p_{r,i+1}/\partial q)$, $J_h = \partial f_d/\partial p_h$, and $\bar{v}_i'(d_i) = d\bar{v}_i(d_i)/dd_i$.

It should be noted that the TV-ZCBF h_i constrains the human's approaching velocity towards the robot's i-th link only. To achieve human safety regarding the robot's whole body, a set of TV-ZCBFs should be defined

$$h_s(x,t) = \big[h_1(x,t), \cdots, h_{n_r}(x,t)\big]^T \in \mathbb{R}^{n_r} \tag{23}$$

Then, the safety control set that guarantees human safety is

$$\mathcal{T}_s = \{\tau \in \mathcal{T} \mid A_s\tau + a_s \geq 0\} \tag{24}$$

where $A_s = [{A_1}^T, \cdots, {A_{n_r}}^T]^T$, and $a_s = [a_1, \cdots, a_{n_r}]^T$.

Assumption 1: The safety control set $\mathcal{T}_s$ is non-empty, i.e., $\mathcal{T}_s \neq \emptyset$.

Remark 1: The above assumption requires the human to move smoothly in the workspace. Otherwise, for instance, when the human moves very fast (i.e., $\|\dot{p}_h\| \to \infty$) toward the robot, the robot may not be able to escape the human fast enough due to the saturated control inputs. In this case, the safety control set $\mathcal{T}_s$ is empty and *Assumption 1* does not hold. This issue is a limitation of the proposed framework. It can be possibly solved by relaxing the safety constraints based on the understanding of the human's intention in future work.

C. Unified Task Control Set for Robot Task

First, the desired behavior of the robot's EE in both contactless and physical HRC modes is described by a mass-spring-damper system activated by the human's force F_h

$$K_m\ddot{e} + K_d\dot{e} + K_p e = F_h \tag{25}$$

where $e = p_e - p_d$ is the tracking error, and K_m, K_d, and K_p are constant positive definite gain matrices. In contactless HRC, $F_h = 0$, so the tracking error e converges to zero. In physical HRC, the robot interacts with the human like a mass-spring-damper system. When (25) is achieved, the robot can switch smoothly between the two HRC modes. Therefore, we design a control set to achieve (25). Note $\ddot{e} = \mathcal{L}_g\mathcal{L}_f p_e \cdot u + \mathcal{L}_f^2 p_e - \ddot{p}_d$, the control set can be designed as follows

$$\mathcal{T}_t = \{\tau \in \mathcal{T} \mid A_t\tau + a_t = 0\} \tag{26}$$

where $A_t = \mathcal{L}_g\mathcal{L}_f p_e$ and $a_t = \mathcal{L}_f^2 p_e - \ddot{p}_d + {K_m}^{-1}(K_d\dot{e} + K_p e - F_h)$. Substituting f and g into the Lie deriavatives, we have $\mathcal{L}_g\mathcal{L}_f p_e = J_v M^{-1}$ and $\mathcal{L}_f^2 p_e = -J_v M^{-1}(C\dot{q} + G - {J_v}^T F_h - {J_\omega}^T T_h) + \dot{J}_v\dot{q}$. The control set $\mathcal{T}_t$ in (26) renders (25) regardless of the HRC mode, so it is called the unified task control set.

The HRC mode at each time step is determined as follows

$$\varphi = \begin{cases} 0, & \|F_h\| < \varepsilon_F \\ 1, & \|F_h\| \geq \varepsilon_F \end{cases} \tag{27}$$

where φ represents the HRC mode ($\varphi = 0$ in contactless HRC mode and $\varphi = 1$ in physical HRC mode), and ε_F is a threshold. The robot works in the contactless HRC mode initially. When $\|F_h\|$ exceeds the threshold ε_F, the robot enters physical HRC mode. In this mode, the desired trajectory p_d should be changed toward the goal position p_g of the human. To this end, p_d is modified as follows

$$\dot{p}_d = K_F F_h \tag{28}$$

where K_F is a constant gain matrix. To obtain the acceleration $\ddot{p}_d$ required in the unified task control set $\mathcal{T}_t$, the measured force F_h is processed by a Kalman filter [3] to estimate its derivative $\dot{F}_h$. When $\|F_h\|$ reduces below the threshold ε_F, the robot returns to contactless HRC mode. In different HRC modes, the unified task control set $\mathcal{T}_t$ is used, and the only difference is that the desired trajectory p_d is modified in the physical HRC mode. The unified task control set $\mathcal{T}_t$ renders (25), thereby achieving a smooth switch of HRC mode.

Theorem 2: Consider the robot model (1) and the human model (4), any controller τ: $\mathbb{R}^{n_x} \to \mathcal{T}_t$ leads to the following:

1) In contactless HRC, the robot's EE p_e tracks the desired trajectory p_d.

2) In physical HRC, when the desired trajectory is modified according to (28), the robot's EE p_e converges to the human's goal position p_g.

Proof: A controller $\tau \in \mathcal{T}_p$ leads to (25). In contactless HRC, $F_h = 0$, so e converges to zero and the first result is proved. In physical HRC, define a positive definite function

$$V_t = \dot{e}^T K_m \dot{e}/2 + e^T K_p e/2 + (p_e^T - p_g^T) K_{hP} (p_e - p_g)/2$$

Note (4), (25), and (28), the time derivative of V_t is

$$\dot{V}_t = -\dot{e}^T K_d \dot{e} - K_F F_h^T F_h - \dot{p}_e^T K_{hD} \dot{p}_e$$

Therefore, we have $F_h \to 0$ and $\dot{p}_e \to 0$, which further leads to $p_e \to p_g$ and $p_d \to p_g$. Then, the second result is proved. ■

D. Quadratic Program

The safety constraints related to human safety are more important than the robot's task. Therefore, $\tau \in \mathcal{T}_s$ should be fulfilled first, while $\tau \in \mathcal{T}_t$ can be fulfilled when possible. Further, there may be some additional constraints to be ensured prior to the robot's task. For instance, when the robot is transporting a cup of water, the EE's orientation should be sustained at all times to avoid water spilling, while the robot's task can be temporarily suspended. A vector $\sigma(x, t) \in \mathbb{R}^{n_\sigma}$ is used to denote the additional constraints, where n_σ is the number. The constraints are fulfilled when $\sigma = 0$, and the following constraint control set is formulated to achieve it

$$\mathcal{T}_c = \{\tau \in \mathcal{T} \mid A_c \tau + a_c = 0\} \tag{29}$$

where $A_c = \mathcal{L}_g \mathcal{L}_f \sigma \in \mathbb{R}^{n_\sigma \times n}$ and $a_c = (\partial/\partial t + \mathcal{L}_f)^2 \sigma + K_{od} \dot{\sigma} + K_{op} \sigma \in \mathbb{R}^{n_\sigma}$ with K_{od} and K_{op} being constant gain matrices. The following QP is employed to coordinate the three control objectives, namely, the robot's task, the safety constraints, and the additional constraints

$$\tau = \arg\min_{\tau} \|A_t \tau + a_t\|^2, \quad \text{s.t.} \quad \tau \in \mathcal{T}_s \cap \mathcal{T}_c \tag{30}$$

Next, we discuss the existence of the solution to the above QP.

First, let us consider the case in which no safety constraint is activated, which means $\mathcal{T}_s = \mathcal{T}$. In this case, the robot should be able to conduct its task while fulfilling the additional constraints, which requires $\mathcal{T}_t \cap \mathcal{T}_c \neq \emptyset$. Generally, this is possible when the robot has enough DOFs, i.e.,

$$n \geq n_t + n_\sigma \tag{31}$$

The robot's task in 3D requires $n_t = 3$ DOFs, and the additional constraints require n_σ DOFs. When (31) holds, the n-DOF robot can achieve the two objectives simultaneously; otherwise, the robot's task will fail since $\mathcal{T}_t \cap \mathcal{T}_c = \emptyset$.

When one or more safety constraints are activated, i.e., $\mathcal{T}_s \subset \mathcal{T}$, the situation becomes rather complicated. In this case, the robot's task can be suspended while the safety constraints and the additional constraints should be fulfilled, which requires the following assumption to hold.

Assumption 2: The intersection of the safety control set $\mathcal{T}_s$ and the constraint control set $\mathcal{T}_c$ is non-empty, i.e., $\mathcal{T}_s \cap \mathcal{T}_c \neq \emptyset$.

Remark 2: The above assumption depends on the human's behavior. When the human is hostile to the robot, the above assumption may not hold. For instance, when the human's two hands approach a link of the robot from opposite directions, the robot may not be able to escape without violating the additional constraints due to the geometric contradiction. Then, the assumption does not hold. In practical applications, the human and the robot are in cooperation rather than opposition, so such cases seldom occur. To tackle the human's hostile behavior, an estimation of the human's intention is necessary, which will be addressed in our future work.

This letter considers a 6-DOF robot manipulator (i.e., UR5e), which allows $n_\sigma = 3$ according to (31). Therefore, the following additional constraints are adopted to make the EE's orientation $R_e \in SO(3)$ track a desired trajectory $R_d \in SO(3)$

$$\sigma(x, t) = e_o = f_o\big(R_e(x) R_d^T(t)\big) \tag{32}$$

where $e_o \in \mathbb{R}^3$ represents the orientation error between R_e and R_d, and the function f_o: $SO(3) \to \mathbb{R}^3$ extracts the vector part of a unit quaternion $\{\eta_o, e_o\}$ corresponding to the input rotation matrix. Substituting σ in (32) into the formulas of A_c and a_c, we have $A_c = E J_\omega M^{-1}$, $a_c = -E J_\omega M^{-1}(C\dot{q} + G - J_v^T F_h - J_\omega^T T_h) + (E\dot{J}_\omega + \dot{E} J_\omega)\dot{q} - (E\dot{\omega}_d + \dot{E}\omega_d) + K_{od}\dot{e}_o + K_{op} e_o$, where ω_d is the angular velocity corresponding to $R_d(t)$ and $E = (\eta_o I_3 - [e_o]_\times)/2$ with $[e_o]_\times$ the skew-symmetric matrix extracted from e_o such that $e_o \times \bullet = [e_o]_\times \bullet$, $\forall \bullet \in \mathbb{R}^3$. The constraint σ in (32) is only an example, other constraints can be defined to achieve, e.g., an admittance control of the EE's orientation.

E. Proposed Control Framework

The schematic diagram of the proposed control framework is shown in Fig. 4(a). The framework aims to provide a control signal for the robot to achieve dual-mode HRC. The control signal consists of the torque inputs τ for the robot's joints and a Boolean variable u to control the gripper that works as the robot's EE. The gripper closes when $u = 1$ and opens when u

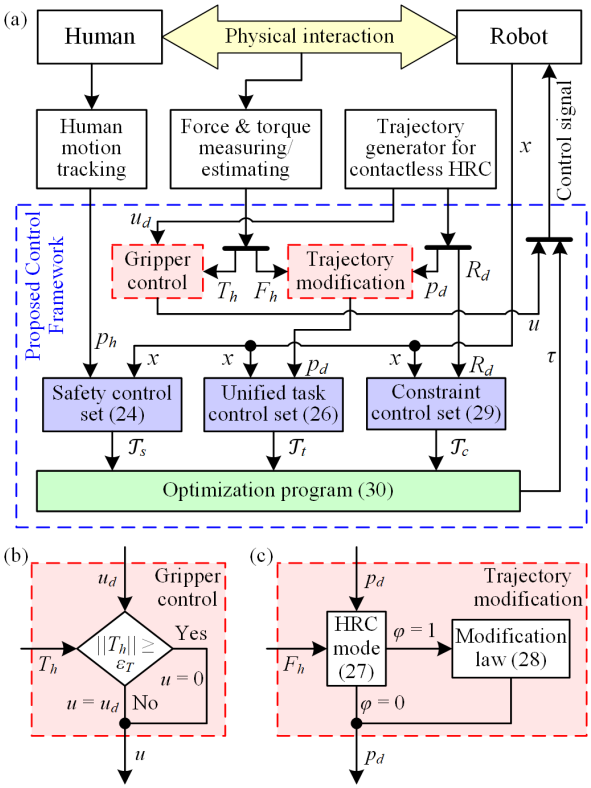

Fig. 4. Schematic diagram of proposed control framework. (a) Proposed control framework. (b) Gripper control. (c) Trajectory modification.

= 0. In practical applications, the framework needs to work together with the following three elements: 1) a human motion tracking system to track the motion of the human represented by p_h, 2) a force and torque sensor/estimator to provide the interaction force F_h and torque T_h between the human and robot, and 3) a trajectory generator to generate the desired trajectory p_d and R_d, as well as the desired operation u_d of the gripper, according to the robot's task in contactless HRC.

Next, we introduce what the proposed framework does at each time step. First, it determines the current HRC mode φ according to (27). When φ = 1, the robot enters physical HRC mode, in which the desired trajectory p_d is modified according to (24). Otherwise, the robot stays in contactless HRC mode with p_d unmodified. Next, the safety control set $\mathcal{T}_s$ for human safety is calculated based on the human motion p_h and the robot state x, the unified task control set $\mathcal{T}_t$ for different robot tasks is calculated based on the desired trajectory p_d and the robot state x, and the orientation control set $\mathcal{T}_c$ for the EE's orientation is calculated based on the desired orientation R_d and the robot state x. Finally, the QP (30) is solved at a frequency of 100 Hz using the method in [22] to obtain the final control input τ. The method in [22] uses a primal-dual neural network based on linear variational inequality to solve a general QP like (30) online. The control signal u sent to the robot is determined by comparing $\|T_h\|$ with a threshold ε_T.

IV. Experiments

A. Experimental Setup

The experimental setup in Fig. 5 is used. It consists of a 6-DOF robot manipulator (UR5e, Universal Robots) equipped with a gripper (2F-85, ROBOTIQ), a LiDAR camera (L515, Intel RealSense), and a computer with a CPU (W-2123 @3.60 GHz, Intel Xeon). The human wears a glove with an ArUco marker. The LiDAR camera tracks the motion of the ArUco marker as the human's motion p_h. As shown in Fig. 5(b), the commercial UR5e robot is integrated with force and torque sensors and an internal joint-velocity controller. The sensors measure the interaction force F_h and torque T_h with the human. The controller generates a joint torque control input $\tau_I \in \mathbb{R}^6$ for the robot so that the actual joint velocity $\dot{q}_I$ track the command $\dot{q}_{\text{cmd}}$. The internal joint torque τ_I of the UR5e robot is not accessible by the users, so we use the proposed control framework to control a virtual UR5e robot based on (1) instead of the real robot. The mass and inertia parameters of the virtual robot are obtained from [23] and are assumed to be close to the real robot. If the state of the real robot tracks the state of the virtual robot, i.e., $x_I = x$, where $x_I = [{q_I}^T, {\dot{q}_I}^T]^T$ with q_I and $\dot{q}_I$ the joint position and velocity of the real UR5e robot, the dual-mode HRC can be achieved in the real world. To this end, the following joint-velocity command is sent to the internal controller of the real UR5e robot at 100 Hz

$$\dot{q}_{\text{cmd}} = \dot{q} + K_q(q - q_I) \tag{33}$$

where $K_q = 5I_6$ is a constant gain matrix. With the command in (33), the state x_I of the real robot provided by the real robot in real time is found to be able to track the state x of the virtual robot with negligible delay (within 0.05 s).

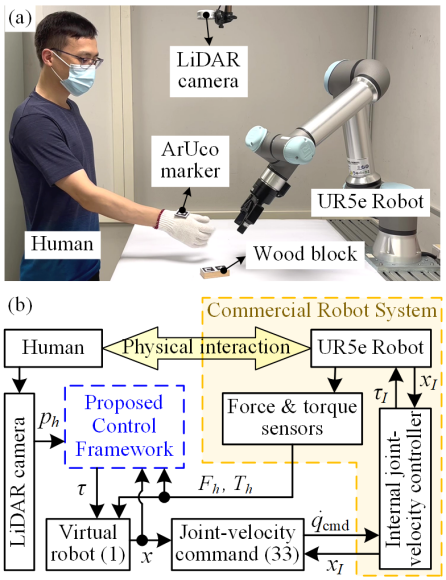

Fig. 5. Experimental setup. (a) Photograph. (b) Sechematic diagram.

TABLE I
Values of Parameters Used in Experiments

Parameters of safety control set	F_c = 140 N, k = 75000 N/m, m_h = 5.6 kg, m_r = 15.4 kg, a_b = 0.18 m/s^2, λ = 10.
Parameters of unified task control set	$K_m = 30I_3$, $K_d = 20I_3$, $K_p = 100I_3$, $K_F = 0.0167I_3$.
Parameters of orientation control set	$K_{od} = 20I_3$, $K_{op} = 100I_3$.
Thresholds	ε_F = 3 N, ε_T = 0.6 N·m.

B. Verification of Proposed Control Framework

First, the human safety is verified. As shown in Fig. 6 and Video 1, when the human approaches the robot gradually so that the approaching velocities v_i regarding different robot links are all above their boundaries $\bar{v}_i$, the robot's EE stays at the desired position. However, when the human approaches the robot rapidly, the robot's EE p_e leaves the desired position p_d to keep the TV-ZCBFs positive. As the human approaches different parts of the robot, the corresponding TV-ZCBF h_i reaches 0. Then, the framework generates an optimal evasive motion for the robot that keeps h_i positive while minimizing the deviation of the EE. As the human stops near the robot, the robot can return to its desired configuration and possibly get into contact with the human. The TV-ZCBFs regarding the four links near the EE are plotted in Fig. 6(a).

Next, the hand-guiding and handover operations are verified. As shown in Fig. 7 and Video 1, when the human's hand approaches the robot's EE, the EE escapes first, then returns, and finally establishes physical contact with the human. After that, the human applies a force F_h to the EE toward the goal position p_g. The framework modifies the desired trajectory p_d according to F_h and make the EE move following the guidance of the human. As a result, the EE can always reach the goal position p_g of the human. When the human applies a torque T_h to the EE, the gripper opens and the human takes the released wood block to achieve a handover.

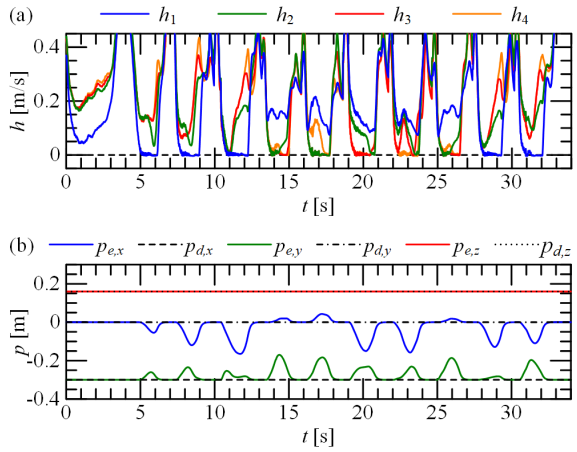

Fig. 6. Verification of human safety. (a) TV-ZCBFs. (b) EE's position.

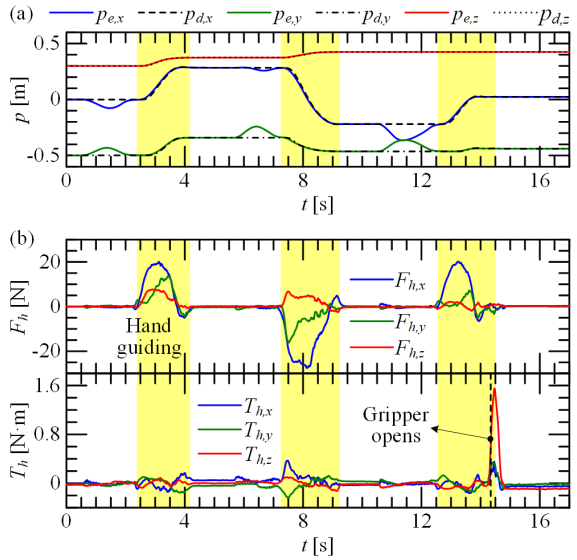

Fig. 7. Verification of hand-guiding and handover. (a) EE's position. (b) Forces and torques.

C. Comparison With Existing Methods

The experiment in Video 2 is designed to compare the proposed control framework with two comparative methods, the control laws of which are given as follows

$$\tau_1 = \arg\min_{\tau} \|A_t\tau + a_t\|^2, \quad \text{s.t.} \quad \tau \in \mathcal{T}_c \tag{33}$$

$$\tau_2 = \arg\min_{\tau} \|A_t\tau + a_t\|^2, \quad \text{s.t.} \quad \tau \in \mathcal{T}_s' \cap \mathcal{T}_c \tag{34}$$

where τ_1 and τ_2 are the control laws of comparative methods I and II, respectively, and $\mathcal{T}_s'$ in (34) is a safety control set of a TV-ZCBF $h' = \dot{p}_e - \bar{v}_e(d_1)$ with $\bar{v}_e$ being the speed limit according to the speed and separation monitoring (SSM) [15]. In both methods, the HRC mode switches according to (27), which is the same as the proposed framework. Compared to the proposed framework based on (30), comparative method I neglects the safety control set $\mathcal{T}_s$, so it simply implements the robot's task without considering human safety, which is the same strategy as [13]. Comparative method II uses a different safety control set $\mathcal{T}_s'$ to implement the SSM defined in the ISO/TS 15066 [15]. The SSM has been adopted by many existing methods [5, 16]. In SSM, the robot can operate at full speed when the human-robot distance is large enough but

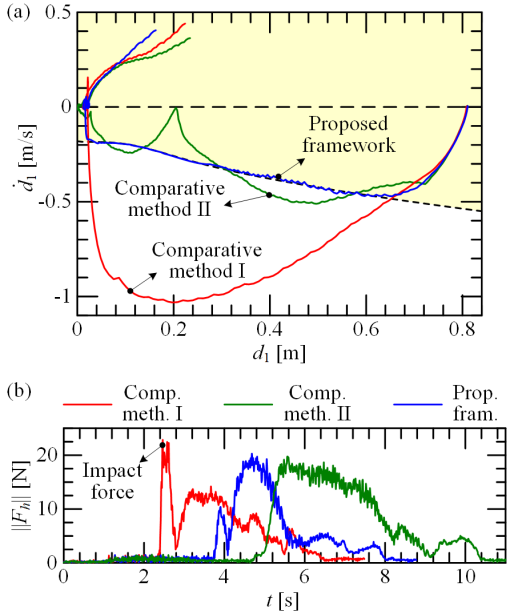

Fig. 8. Comparison of proposed framework with existing methods. (a) Phase portraits. (b) Contact forces.

should reduce its speed and finally stop as the distance decreases. In the experiment, the full speed $\bar{v}_e = 0.5$ m/s can be reached when the distance $d_1 \geq 0.7$ m. As d_1 decreases from 0.7 to 0.2 m, the speed limit $\bar{v}_e$ reduces linearly from 0.5 to 0 m/s. Thus, the robot stops when $d_1 \leq 0.2$ m.

As shown in Video 2, when comparative method I is applied, the robot collides with the human without reducing its speed. As shown in Fig. 8, the approaching velocity exceeds its safe boundary before colliding, resulting in a large impact force that may hurt the human. Comparative method II can slow down the robot as the distance to the human reduces. As the distance falls below 0.2 m, the robot stops and the human has to approach the robot to enter physical HRC mode, which reduces the efficiency of HRC. On the contrary, as indicated by the blue curve in Fig. 8(a), the proposed framework can strictly keep a safe approaching velocity between the human and the robot. As a result, when the human moves toward the robot, the robot can escape backward. When the human stops, the robot can still approach the human under safety constraints to enter physical HRC mode. Then, the efficiency is improved.

D. An Application Example of Proposed Control Framework

An application example of the proposed control framework is presented in Video 3. In this example, the robot picks a stack of wood blocks on the left side of the workbench and places them on the right side one by one. There are ArUco markers on the wood blocks so that they can be located by the LiDAR camera. The human assists the robot in the pick-and-place task. With the proposed control framework, the human can assist the robot in different ways.

The experiment is divided into three phases based on how the human assists the robot. In phase I, the human picks a wood block from the stack and places it in the desired position, while the robot keeps a safe approaching velocity to the human's hand. In phase II, the human intends to change the position to place the wood block. To this end, the human

intercepts the operating robot and guides the EE to the goal position. After the human's hand retracts, the EE places the wood block. In phase III, the human intends to take over the wood block via handover and place it in the desired position. To this end, the human intercepts the robot and applies a torque to the EE so that the gripper opens. Then, the human takes the released wood block and places it on the workbench.

V. Conclusion and Future Work

This letter proposes a control framework to achieve the dual-mode HRC: the robot can perform contactless HRC under safety regulations; while the human can safely interrupt the robot via physical contact to enter physical HRC, in which he/she can hand guide the robot or take over its gripped object. First, human safety is defined as bounded approaching velocities between human and robot links based on ISO/TS 15066, which is further guaranteed by the proposed TV-ZCBF. Second, a unified task control set is designed to achieve different robot tasks in a unified manner, thereby achieving a smooth switch between the two HRC modes. Finally, a QP is employed to determine the final control input.

The proposed framework still has some limitations to be addressed in future work. First, the human safety is restricted to limited contact force resulting from a collision with the robot. Our future work will consider human safety from a larger perspective. Second, the existence of the solution to the QP depends on the assumptions related to the human's behavior. When the human behaves abnormally, e.g., moving too fast for the robot to escape or causing a geometric contradiction with the robot, the assumptions will not hold and the QP will have no solution. New strategies will be developed to handle these cases. Third, the robot's escape behavior may seem to avoid the human's collaboration intention. An estimation of the human's intention will be included in the framework to achieve a more efficient switch of HRC mode.

References

[1] S. Lyu and C. C. Cheah, "Human-Robot Interaction Control Based on a General Energy Shaping Method," *IEEE Transactions on Control Systems Technology*, vol. 28, no. 6, pp. 2445-2460, Nov 2020, doi: 10.1109/tcst.2019.2949525.

[2] M. Khatib, K. Al Khudir, and A. De Luca, "Human-robot contactless collaboration with mixed reality interface," *Robotics and Computer-Integrated Manufacturing*, vol. 67, Feb 2021, Art no. 102030, doi: 10.1016/j.rcim.2020.102030.

[3] F. Ferraguti *et al.*, "Safety barrier functions and multi-camera tracking for human-robot shared environment," *Robotics and Autonomous Systems*, vol. 124, Feb 2020, Art no. 103388, doi: 10.1016/j.robot.2019.103388.

[4] S. J. Moon, J. Kim, H. Yim, Y. Kim, and H. R. Choi, "Real-Time Obstacle Avoidance Using Dual-Type Proximity Sensor for Safe Human-Robot Interaction," *IEEE Robotics and Automation Letters*, vol. 6, no. 4, pp. 8021-8028, Oct 2021, doi: 10.1109/lra.2021.3102318.

[5] A. Pupa, M. Arrfou, G. Andreoni, and C. Secchi, "A Safety-Aware Kinodynamic Architecture for Human-Robot Collaboration," *IEEE Robotics and Automation Letters*, vol. 6, no. 3, pp. 4465-4471, Jul 2021, doi: 10.1109/lra.2021.3068634.

[6] F. Ferraguti, M. Bertuletti, C. T. Landi, M. Bonfe, C. Fantuzzi, and C. Secchi, "A Control Barrier Function Approach for Maximizing Performance While Fulfilling to ISO/TS 15066 Regulations," *IEEE Robotics and Automation Letters*, vol. 5, no. 4, pp. 5921-5928, Oct 2020, doi: 10.1109/lra.2020.3010494.

[7] X. Y. Wu, Z. J. Li, Z. Kan, and H. B. Gao, "Reference Trajectory Reshaping Optimization and Control of Robotic Exoskeletons for Human-Robot Co-Manipulation," *IEEE Transactions on Cybernetics*, vol. 50, no. 8, pp. 3740-3751, Aug. 2020, doi: 10.1109/tcyb.2019.2933019.

[8] H. Zhang, Q. Sheng, J. W. Hu, X. J. Sheng, Z. H. Xiong, and X. Y. Zhu, "Cooperative Transportation With Mobile Manipulator: A Capability Map-Based Framework for Physical Human-Robot Collaboration," *IEEE-ASME Transactions on Mechatronics*, doi: 10.1109/tmech.2022.3155601.

[9] X. B. Yu, W. He, Q. Li, Y. A. Li, and B. Li, "Human-Robot Co-Carrying Using Visual and Force Sensing," *IEEE Transactions on Industrial Electronics*, vol. 68, no. 9, pp. 8657-8666, Sep 2021, doi: 10.1109/tie.2020.3016271.

[10] P. Chang, R. Luo, M. Dorostian, and T. Padr, "A Shared Control Method for Collaborative Human-Robot Plug Task," *IEEE Robotics and Automation Letters*, vol. 6, no. 4, pp. 7429-7436, Oct 2021, doi: 10.1109/lra.2021.3098323.

[11] W. He, J. S. Li, Z. C. Yan, and F. Chen, "Bidirectional Human-Robot Bimanual Handover of Big Planar Object With Vertical Posture," *IEEE Transactions on Automation Science and Engineering*, vol. 19, no. 2, pp. 1180-1191, Apr 2022, doi: 10.1109/tase.2020.3043480.

[12] D. P. Losey and M. K. O'Malley, "Trajectory Deformations From Physical Human-Robot Interaction," *IEEE Transactions on Robotics*, vol. 34, no. 1, pp. 126-138, Feb 2018, doi: 10.1109/tro.2017.2765335.

[13] A. Cherubini, R. Passama, P. Fraisse, and A. Crosnier, "A unified multimodal control framework for human-robot interaction," *Robotics and Autonomous Systems*, vol. 70, pp. 106-115, Aug 2015, doi: 10.1016/j.robot.2015.03.002.

[14] E. Lamon, F. Fusaro, P. Balatti, W. Kim, and A. Ajoudani, "A Visuo-Haptic Guidance Interface for Mobile Collaborative Robotic Assistant (MOCA)," *2020 IEEE/RSJ International Conference on Intelligent Robots and Systems (IROS)*, pp. 11253-11260, 2020.

[15] ISO TS 15066:2016. "Robots and robotic devices – Collaborative robots," Feb. 15, 2016. [Online]. Available: http://www.iso.org

[16] Y. Kang, D. Kim, and D. W. Yun, "Manipulator Collision Avoidance System Based on a 3D Potential Field With ISO 15066," *IEEE Access*, vol. 10, pp. 126593-126602, 2022, doi: 10.1109/access.2022.3221182.

[17] R. Weitschat and H. Aschemann, "Safe and Efficient Human-Robot Collaboration Part II: Optimal Generalized Human-in-the-Loop Real-Time Motion Generation," *IEEE Robotics and Automation Letters*, vol. 3, no. 4, pp. 3781-3788, Oct 2018, doi: 10.1109/lra.2018.2856531.

[18] L. Joseph, J. K. Pickard, V. Padois, and D. Daney, "Online velocity constraint adaptation for safe and efficient human-robot workspace sharing," *2020 IEEE/RSJ International Conference on Intelligent Robots and Systems (IROS)*, pp. 11045-11051, 2020.

[19] A. D. Ames, X. R. Xu, J. W. Grizzle, and P. Tabuada, "Control Barrier Function Based Quadratic Programs for Safety Critical Systems," *IEEE Transactions on Automatic Control*, vol. 62, no. 8, pp. 3861-3876, Aug 2017, doi: 10.1109/tac.2016.2638961.

[20] M. Rauscher, M. Kimmel, and S. Hirche, "Constrained Robot Control Using Control Barrier Functions," *2016 IEEE/RSJ International Conference on Intelligent Robots and Systems (IROS)*, pp. 279-285, 2016.

[21] T. Stouraitis, I. Chatzinikolaidis, M. Gienger, and S. Vijayakumar, "Online Hybrid Motion Planning for Dyadic Collaborative Manipulation via Bilevel Optimization," *IEEE Transactions on Robotics*, vol. 36, no. 5, pp. 1452-1471, Oct 2020, doi: 10.1109/tro.2020.2992987.

[22] D. S. Guo and Y. N. Zhang, "Acceleration-Level Inequality-Based MAN Scheme for Obstacle Avoidance of Redundant Robot Manipulators," *IEEE Transactions on Industrial Electronics*, vol. 61, no. 12, pp. 6903-6914, Dec 2014, doi: 10.1109/tie.2014.2331036.

[23] Universal Robots, *DH Parameters for Calculations of Kinematics and Dynamics*. Online available: https://www.universal-robots.com/articles/ur/application-installation/dh-parameters-for-calculations-of-kinematics-and-dynamics/